

RECENT ASTRONOMICAL RESULTS FROM
THE INFRARED SPATIAL INTERFEROMETER
AND THEIR IMPLICATIONS FOR LOUISA

W.C. Danchi, M. Bester, and C.H. Townes

Space Sciences Laboratory and Physics Department
University of California at Berkeley
Berkeley, CA 94720 USA

Abstract

A new heterodyne interferometer for the atmospheric window from 9-12 μm has been developed at the University of California at Berkeley during the past five years. This instrument, called the Infrared Spatial Interferometer (ISI), has been designed to use earth rotation aperture synthesis techniques developed in radio interferometry. It was moved to Mt. Wilson, California, in January 1988 and first fringes were obtained in June of that year. Systematic observations of some of the brighter late-type stars began shortly after the first fringes were obtained. We describe the basic principles and design of the ISI and give an overview of some of the initial results obtained from these observations. The implications of our work to the proposed Lunar Optical/UV/IR Synthesis Array (LOUISA) are discussed. We also analyze the conditions for the maximum signal-to-noise ratio of such an interferometer as a function of wavelength. The optimum wavelength is found to depend on the assumed scaling relation between telescope area and wavelength.

Introductions and ISI Design

During the 1970s our group developed and obtained astronomical results with a prototype heterodyne interferometer operating in the spectral window from 9-12 μm . This instrument had a fixed 5.5 m east-west baseline and demonstrated the fundamental principles of long-baseline interferometry in the mid-infrared (Johnson et. al. 1974). Based on the experience with this prototype instrument, we have designed and constructed a new interferometer using portable large-aperture telescopes of a novel design.

Figure 1 displays a schematic view of such a portable telescope, which we call a Pfund telescope. A 2.03 m diameter flat mirror supported on an altitude-azimuth mount is used to track an astronomical source. Light is reflected by the flat mirror onto a 1.65 m diameter parabolic mirror. This mirror focuses the light to a point behind the flat mirror. A dichroic mirror separates the infrared and optical signals. The optical light is used for guiding while the infrared radiation is mixed with radiation from a CO₂ laser, and is detected on an HgCdTe photodiode. The resulting intermediate frequency (IF) heterodyne signals from the two telescopes are processed using conventional radio techniques to find the interference fringes.

The choice of telescope geometry allows for a range of $\pm 55^\circ$ in azimuthal rotation angle from the position where the flat mirror points directly at the parabola, and for a range from -2° to $+55^\circ$ in altitude, with twice this angular range on the sky. Therefore the sky coverage is about half of the visible sky. Unlike conventional alt-az mounts, the Pfund mount has no singularity at the zenith. Another advantage of this geometry aside from compactness is that it has no support struts for a secondary mirror, which usually give rise to diffraction effects and partly block the aperture. One disadvantage is limited sky coverage, but this can be overcome by rotating the trailers by 180° .

The mounts for both mirrors are kinematically supported on reinforced concrete bases. The mirrors, detection optics, control system, and computer system are all contained within the custom-made semi-trailers. The current site has seven stations with east-west baselines ranging from 4 to 28 m and north-south baselines of up to 15 m, as well as baselines at intermediate angles. Normally the semi-trailers are mechanically decoupled from the mirror mounts, but to change baselines, a trailer is raised to carry the weight of the mirror mounts, driven to a new station, and then lowered to release the mirror mounts.

Pathlengths within each telescope itself are monitored by a HeNe laser metrology system indicated in figure 1 by the dot-dashed lines between the flat and parabolic mirrors. The position of the center of rotation of the flat mirror can be monitored with respect to bedrock by triangulation from a monument located near the trailer tires shown in the figure. The baseline length and orientation can then be monitored, assuming the bedrock is fixed and the monuments are thermally shielded and isolated from wind shaking. (cf. Townes 1984; Townes et al. 1986; Danchi et al. 1986).

Precise pointing is achieved using conventional incremental optical encoders with a resolution of about 0.24 arc sec in azimuth and 0.07 arc sec in altitude on the sky. This system has a blind pointing accuracy of less than 10 arc sec (rms) in azimuth and less than 2.5 arc sec (rms) in altitude on the sky. In the near future we expect to use laser metrology to directly measure the pathlengths between the two mirrors and, hence, the relative angle. This system has a theoretical precision of 0.008 arc sec on the sky, but atmospheric effects are expected to lower it to a practical precision of about 0.1 arc sec. (See also discussion by Danchi et al. 1986.)

The ISI uses a heterodyne detection technique much like that of the basic radio interferometer shown schematically in figure 2. In the heterodyne interferometer, a local oscillator signal and a signal from an astronomical source are mixed together. The result is the down-conversion of the sky signal into the IF band. A phase shifter can be used to adjust the relative phase (or frequency) between the two antennas which make up the interferometer. This allows one to compensate for the varying frequency of the interference signal due to the changing projected baseline resulting from the earth's rotation (lobe rotation). The chief advantage of the heterodyne technique is that the interference can occur at the IF band, which allows a greatly relaxed tolerance for the delay line, a device which compensates for the varying phase delay across the IF band resulting from the geometrical delay. In this way one obtains a "white light" fringe. At millimeter and centimeter wavelengths, the IF signals are quite often digitized so that both the delay and correlation can be achieved in digital correlators.

One major difference between a mid-infrared heterodyne interferometer and a typical centimeter or millimeter wavelength interferometer (which also uses heterodyne detection) is that the IF band for the IR interferometer must be much larger by comparison to obtain reasonable sensitivity. Thus our IF banks is as large as is reasonably practical (0.2-2.0 GHz). Instead of using a digital delay and correlation technique, we find that it is easier to use an analog delay line and a multiplying correlator. Other differences occur because of the short wavelength involved. One is that the local oscillator used in the mid-IR is a stable CO₂ laser rather than a solid-state source such as a Gunn diode. Another difference is that the local oscillator and signal beams are combined optically on a ZnSe beamsplitter and are then focused onto a cooled HgCdTe photodiode (Spears 1977). Rather than using a single local oscillator and a phase shifter, we use two CO₂ lasers, one in each telescope. One laser is free-running. A part of the output from this laser is sent from one optic's room through an air path between the telescopes to the optic's room of the second telescope, where it is mixed with the second laser beam. Then this laser is phase locked

to the first one to provide the correct phase and frequency difference between the two telescopes. The frequency difference between the lasers is chosen to compensate for the natural fringe frequency which varies due to the change in the projected baseline resulting from the rotation of the earth. We use a fixed fringe frequency of 10 Hz, which is sampled by an analog-to-digital converter at a rate of 100 Hz. Techniques used to ensure phase stability of the local oscillator signals between the two telescopes are somewhat similar to those used in radio interferometry (Thompson et al. 1986). A portion of the CO₂ laser beam, which is sent between the telescopes, is returned along the same path. The returned beam is mixed with a part of the original laser beam and the resulting interference fringes are used to measure the relative phase of the two beams. A constant round-trip phase is maintained by a simple servo loop controlling a variable pathlength device inserted in the optical path between the telescopes. More detailed discussions of the ISI detection system have been published elsewhere (Danchi et al. 1988).

Sensitivity is a major disadvantage of the heterodyne technique, particularly at shorter wavelengths (for continuum sources). Generally speaking, the heterodyne technique is favored for narrow bandwidths or when the background is large. Direct detection is preferred for large bandwidths and low backgrounds. (See for example Kingston 1978 and Burke 1985.) The ISI is estimated to obtain satisfactory signals from sources about six magnitudes weaker than the brightest 10 μ m infrared sources using realistic assumptions about bandwidths, quantum efficiencies, integration, and atmospheric coherence times (Danchi et al. 1988).

We turn now to some of the results from our initial series of observations with the ISI.

Recent Astronomical Results

The ISI reached two major milestones during the 1988 observing season. One was the detection of the first interference fringes on 29 June 1988. The other was the initiation of the observational program. Thus far one dozen of the brighter 10 μ m infrared sources have been observed. These sources were IRC+10216, VY CMa, α Ori, α Sco, σ Ceti, R Leo, VX Sgr, W Aql, χ Cyg, R Aqr, α Tau, and U Ori. The brightest source observed was the much studied carbon star IRC +10216 (CW Leo) with a flux of about 25,000 Jy; the weakest sources were α Tau and U Ori, each with a flux of about 700 Jy. (Here 1 Jy = 10^{-26} W m⁻² Hz⁻¹.) During the 1988 observing season, we spent most of our time installing and debugging the telescopes, the pointing system, and the

detection system. The data which we will discuss here were obtained in a total of about one week of observing during a period of excellent seeing.

Figure 3 displays the power spectrum of the fringe signal on IRC +10216 obtained over a 512 second integration time. This figure was obtained by coadding 25 power spectra, each one obtained from a separate 20.48 second time section of the sampled data. Note that the spike occurs at the expected fringe frequency of 10 Hz. Note also the wings on the fringe extending to about 1 Hz on either side of the 10 Hz fringe signal. The wings on the fringe signal are due to fluctuations in the pathlengths from the star to the telescopes caused by turbulence in the atmosphere as well as perhaps by some wind shaking or mechanical vibrations in the telescope mounts. Turbulence associated with heat sources internal to the telescopes could also contribute to these pathlength fluctuations.

Another way to analyze the data is to calculate the amplitude and phase of the interference signal directly from the time series data. Here one essentially multiplies the fringe signal by $\sin \omega t$ and $\cos \omega t$, where $\omega = 2\pi \cdot 10$ Hz, and integrates over a time period corresponding to at least a few cycles of the 10 Hz waveform. The result of this computation on a portion of the data on IRC +10216 is shown in figure 4. Here we display the power in telescopes 1 and 2 as a function of time in seconds beginning at an arbitrary starting time, and the fringe phase and amplitude, using a 0.2 second integration time. The fringe phase is displayed in degrees and the fringe amplitude is shown in arbitrary units. The fringe phase clearly fluctuates from its mean value to an extremum and returns to approximately the main value again over a period of a few seconds. Such time scales are not surprising because the Mark III visible wavelength interferometer observed a Fried coherence diameter (r_0) of about 19 cm at $0.55 \mu\text{m}$ for an effective wind speed of 14 m sec^{-1} during a period of good seeing (Colavita et al. 1987). From these values one would expect the fringe phase to change by about one radian in about 0.5 sec. Thus a complete cycle of fluctuation should take a few seconds. Averages over periods of a few minutes will greatly decrease fluctuations and provide quite accurate phase measurements.

The power spectrum of fringe phase or pathlength fluctuations can be calculated from data similar to those in figure 4. A power spectrum has been calculated for some of the IRC +10216 data taken on 8 October 1988 and is displayed in figure 5. Two pieces of data were analyzed, each about 2.5 minutes in length. The data in figure 5 cover the frequency range from about 25 mHz and can be fit by a power law in frequency $P_L(\nu) \propto \nu^{-\alpha}$, where α can be fit to values between 1.3 and 1.5.

This power spectrum can be compared to that obtained with the Mark III interferometer (Colavita et al. 1987). Their data were fit by a low frequency asymptotic power law of the form $P_L(v) = C_1 B^2 v^{-2/3}$ for $v \ll v/B$, where B denotes the baseline length and v the wind speed. For frequencies such that $v \gg v/B$, their data were fit by a power law of the form $P_L(v) = C_2 v^{-8/3}$. Both asymptotic power law formulae can be derived from the Kolomogorov turbulence theory as has been discussed by Colavita et al. (1987).

To make a comparison with the Mark III data, one must scale the cross-over frequency (where the power law changes from the $-2/3$ to the $-8/3$ power) with the baseline length ratio. This scaling must be made because our data were taken with a 4 m baseline while the data of Colavita et al. were taken with a 12 m baseline. If we define f_1 to be the cross-over frequency for baseline B_1 and if f_2 is the cross-over frequency for baseline B_2 then $f_2 = (B_1/B_2)f_1$ because the cross-over frequency $f = (C_2/C_1)^{1/2} B^{-1}$. For pathlength fluctuations, power on the low frequency asymptote scales as the baseline ratio squared, i.e., $(B_2/B_1)^2$. When we scale the low-frequency asymptote and the cross-over frequency with the baseline from figure 7 of Colavita et al., we find that the agreement between the two data sets is excellent. Figure 5 displays the scaled asymptotes from figure 7 of Colavita et al. The low frequency asymptotes ($v^{-2/3}$) are indicated by the dot-dashed line in the figure and the high frequency asymptotes ($v^{-8/3}$) are drawn as the dotted line. Our data tend to lie slightly below their asymptotic power law, but this variation could easily be due to differences in the projected baseline between the two systems and source as well as the airmass. Note that their figures 6, 7, and 8 are all consistent with each other when one takes the variation in baseline length or airmass into account. For example, the data in figure 8 were taken with a baseline length of 3.1 m on the Mark II system while the data in figures 6 and 7 were taken with the 12-m baseline of the Mark III system. One would expect the low frequency asymptote of their figure 8 to lie $(12/3.1)^2$, or about 12 dB below that of figure 6 or 7, which is approximately what is observed. We must caution the reader that the analysis presented here is preliminary; more detailed analysis will be published elsewhere after further observations. The analysis presented here shows that coordinated observations of the same source observed simultaneously with both the visible and IR interferometers on Mt. Wilson could prove useful in identifying contributions from wavelength dependent fluctuations such as is expected from water vapor.

One further aspect of the current data set deserves a brief mention here. The visibilities of some of the observed sources can be computed from a comparison between the observed power in the interference fringes and the flux in a single telescope. Figure 6 displays an intercomparison

between the fluxes of three bright IR stars and the power in their interference fringes. Note that the single telescope flux for VY CMa lies about a factor of two above that for α Ori, whereas the power in the fringes for α Ori lies about a factor of five above the VY CMa. Thus, we must resolve VY CMa more than α Ori. Similarly the single telescope flux for IRC+10216 is about a factor of nine larger than that for α Ori, although the fringe powers vary by only about a factor of four. We can see that the ISI has the potential for accurate measurements of the fringe amplitudes and phases. Once these measurements are sufficiently accurate, one of the early scientific goals of the IR interferometer will be to determine the spatial distribution of dust around some of the brighter late-type stars. Such measurements should have important consequences for the study of the mass-loss phenomena of these stars.

Implications For The LOUISA Concept

In an interesting paper from the Conference on Lunar Bases and Space Activities of the 21st Century, Burke (1985) put forth a set of arguments in support of the construction of a Lunar Optical/UV/Infrared Synthesis Array (LOUISA). An obvious advantage of the Moon-based interferometer as compared to an Earth-based one is the lack of an atmosphere that causes fluctuations in the phase of the interference fringes and which is a primary limitation of interferometry on the Earth's surface. Clearly the low surface gravity would make it possible to build telescopes from lightweight structures. Also the stable soil would make an easy platform from which one might point and control the attitude of the individual telescopes as well as maintain the baseline orientation.

For the first interferometer built on the Moon, it is clearly appropriate to build a system for wavelengths shorter than the $10\ \mu\text{m}$ used for the ISI and to use direct detection rather than heterodyne techniques. However, some of the ISI experience, perhaps particularly with HeNe interferometer monitoring of distances for precision under varying conditions, should be of value in considering such a system.

An important question that has received relatively little attention with regard to the LOUISA concept is that of the optimum wavelength for the proposed interferometer array. One might envision that discussions could be based on a well-defined set of criteria, for example the signal-to-noise ratio, or on the ease of construction based on optical fabrication or alignment tolerances. It is also useful to consider weight limitations based on transportation costs, or a clearly defined set of scientific goals which are achievable for particular wavelength regimes. It

is difficult to judge what particular design considerations should be made for an instrument that would be expected to be in operation 20-25 years in the future or even what the most important scientific problems will be in the next century. One set of criteria that will most likely not change significantly with time is that of the signal-to-noise ratio. Here we present some simple arguments that suggest a compromise toward longer wavelengths than have been discussed so far.

We assume that there are detectors available that essentially count photons over the wavelength range from 0.5 to 5.0 μm . We are not suggesting that any single detector would cover that range but that there are detector technologies available to cover it. Photon-counting detectors for longer wavelengths may be available by the time a lunar base exists, but for now we ignore this possibility. Consider now a blackbody source of temperature T . Then, at a frequency ν , the Planck, function is given by

$$B_{\nu}(T) = \frac{2h\nu^3/c^2}{e^{h\nu/kT} - 1}, \quad (1)$$

where B_{ν} has units of $\text{W m}^{-2} \text{Hz}^{-1} \text{ster}^{-1}$. For a given frequency band $\Delta\nu$, which is some fixed fractional bandwidth of the frequency ν , the number of photons per unit time collected by a hypothetical telescope of area A can be shown to be

$$\Gamma_{\text{coll}} = \frac{\kappa\nu^3 A}{e^{h\nu/kT} - 1}, \quad (2)$$

where κ is a constant of proportionality, Let A be a free parameter that may also be scaled with frequency ν according to a power law $A = \gamma\nu^{-n}$, where for the purposes of this discussion we restrict n to be a positive integer or zero. In fact the empirically correct scaling law between telescope area and frequency may not be a simple integer power of the frequency. If we transform to the dimensionless variable $x \equiv h\nu / kT$, we obtain

$$\Gamma_{\text{coll}} = \frac{\gamma\kappa(kT/h)^{3-n} x^{3-n}}{e^x - 1}. \quad (3)$$

The basic idea in scaling the antenna area with frequency is that in almost any conceivable design, there is a compromise between design tolerance such as surface accuracy and telescope

size. A more precise mirror suitable for short wavelengths would generally be smaller than one for longer wavelengths where less precision is needed. It is also generally true that, for a given precision, the total telescope weight scales approximately as the cube of its diameter. So there is a sensible trade-off between telescope area and wavelength up to the point when the total payload weight becomes intolerably large. Thus one expects the suggested scaling law to be valid over a limited frequency range. The specific mirror fabrication technology chosen may determine the relevant area-frequency power law, but one would expect it to be in the range of the three choices $A = \text{const}$, $A \propto \nu^{-1}$, or $A \propto \nu^{-2}$.

A simple physical argument can be used to show why one would expect the area to scale approximately as a simple inverse integer power of frequency. As had been noted by Burke (1985), the deflection s of a beam can be written as

$$s \approx \gamma(\rho/Y) g_m l^2, \quad (4)$$

where s depends on the length of the beam l , on the gravitational constant, g_m , on the Young's modulus Y , on the density ρ , and on the dimensionless geometrical factor γ . If the fractional error tolerance for the mirror is independent of frequency, for example, one usually expects to have a mirror with an rms surface accuracy of $\lambda/10$ or better, where λ is the wavelength; the allowable deflection s would then also be proportional to wavelength, or inversely proportional to frequency. Hence from equation (4), $l^2 \propto \nu^{-1}$, which implies $A \propto \nu^{-1}$. Similar arguments can be constructed for the situation where forces, other than those due to gravity, are distorting the mirror. These forces would tend to give rise to scaling laws within the range encompassed by the integer power law indices 0, 1, and 2.

Figure 7 displays the signal-to-noise ratio in terms of the number of photons collected per second with an arbitrary scale factor as a function of the scaled variable x . The solid curve shows Γ_{coll} for the case when $A = \text{const}$; the short dashed curve is for the case when $A \propto \nu^{-1}$, while the long dashed lines represent a curve for $A \propto \nu^{-2}$. One fact that becomes immediately apparent from these curves is that the maximum value of $\Gamma_{coll}(x)$ is shifted to a lower value of x as n increases. If telescope area is very inexpensive to add, such as when $A \propto \nu^{-2}$, then for a fixed temperature T one is driven toward very low frequencies, indeed to $\nu = 0$. If $A \propto \nu^{-1}$ then Γ_{coll} peaks at $x_{\text{max}} = 1.6$ as compared to the constant area case where $x_{\text{max}} = 2.8$. This suggests an optimum wavelength modestly longer than that suggested by the constant area curve. If we pick a particular frequency,

we can investigate how the signal-to-noise changes with temperature. If we choose a wavelength of $1\ \mu\text{m}$, then the signal-to-noise ratio drops by only a factor of 2 for temperatures between 2,700 K and 12,000 K, as can be determined from the solid curve, i.e., the blackbody curve. The maximum occurs near 5,000 K.

This choice of optimum wavelength allows one to be sensitive to stellar spectral types from the cool M5 dwarfs all the way to hot B5 stars, which covers most of the main sequence as well as most of the red giant branch. Extinction due to interstellar dust is much less at $1\text{-}2\ \mu\text{m}$ than in the visible or UV. For example, some active galactic nuclei, essentially all star-forming regions, the Galactic Center, many late-type stars, and proto-planetary nebulae are enshrouded by dust clouds that are optically thick at visible wavelengths. Clearly the study of these objects would be enhanced by the longer wavelength capability. It may also be useful to consider the construction of more than one array, such as separate arrays, with one optimized for the UV/visible wavelengths, the other for the infrared.

Summary and Conclusions

The Infrared Spatial Interferometer (ISI) is a heterodyne interferometer that operates in the atmospheric window around $10\ \mu\text{m}$. In January 1988 it was installed on Mt. Wilson and the first interference fringes were observed by the ISI in June 1988. An initial data set on a dozen late-type stars was also obtained this observing season, which demonstrated that this interferometer behaves essentially as expected from its design parameters. A preliminary analysis of fringe phase fluctuations shows that the fluctuations are consistent with those observed on the Mark III visible interferometer, also located on Mt. Wilson. The data also demonstrate that high accuracy visibilities can be determined.

We show by simple scaling arguments that a lunar visible/IR synthesis array may be optimized for wavelengths in the near infrared that are somewhat longer than have been proposed previously.

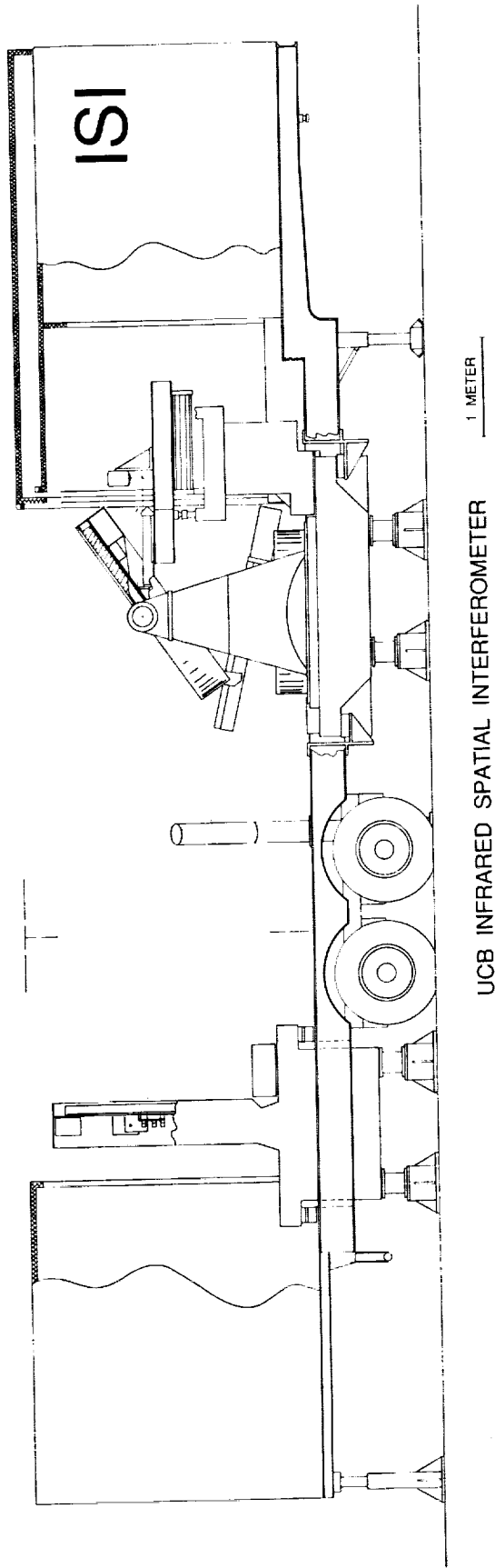
Acknowledgments

We are pleased to thank P. R. McCullough for his assistance with the astronomical observations and data analysis, and for a critical reading of this manuscript. This work was supported in part by the U.S. Office of Naval Research Contract No. N00014-82-C-0700 and grants

from the California Space Institute and the Perkin Fund. One of the authors (WCD) has been supported in part by the L. W. Frohlich Research Fellowship of the New York Academy of Sciences.

References

1. Burke, B. F. 1985. Conference on Lunar Bases and Space Activities of the 21st Century, Lunar and Planetary Institute, Houston, TX, 73.
2. Colavita, M. M.; Shao, M.; Staelin, D. H. 1987. Appl. Optics, 26:2106.
3. Danchi, W. C.; Arthur, A.; Fulton, R.; Peck, M.; Sutton, E. C.; Townes, C. H.; Weitzmann, R. H. 1986. Proc. of the SPIE Conference on Advanced Technology Optical Telescopes III, 628:422.
4. Danchi, W. C.; Bester, M.; Townes, C. H. 1988. High Resolution Imaging by Interferometry, F. Merkle, ed., ESO Conference and Workshop Proceedings No. 29 (Garching, FRG:European Southern Observatory):867.
5. Johnson, M. A.; Betz, A. L.; Townes, C. H. 1974. Phys. Rev. Lett., 33:1617.
6. Kingston, R. H. 1978. Detection of Optical and Infrared Radiation, (New York: Springer-Verlag), Spears, D. L. 1977, Infrared Phys., 17:5.
7. Thompson, A. R.; Moran, J. M.; Swenson, G. W. 1986. Interferometry and Synthesis in Radio Astronomy (New York: John Wiley and Sons, Inc.):185.
8. Townes, C. H. 1984. J. Astrophys. and Astron., 5:111.
9. Townes, C. H.; Danchi, W. C.; Sadoulet, B.; and Sutton, E. C. 1986. Proc. of the SPIE Conference on Advanced Technology Optical Telescopes III, 628:281.



Danchi et al.

Figure 1: Schematic illustration of one of the Pfund telescopes of the University of California Infrared Spatial Interferometer. Starlight is reflected by the flat mirror on the right of the figure to the parabolic mirror on the left side of the figure. The light is focused by the parabolic mirror through a hole in the flat mirror and is subsequently detected and further processed on an optics table located in a room behind the flat mirror. This mirror is supported by an alt-az mount. The telescope mounts are housed in a standard size semi-trailer and are decoupled from the trailer when observing.

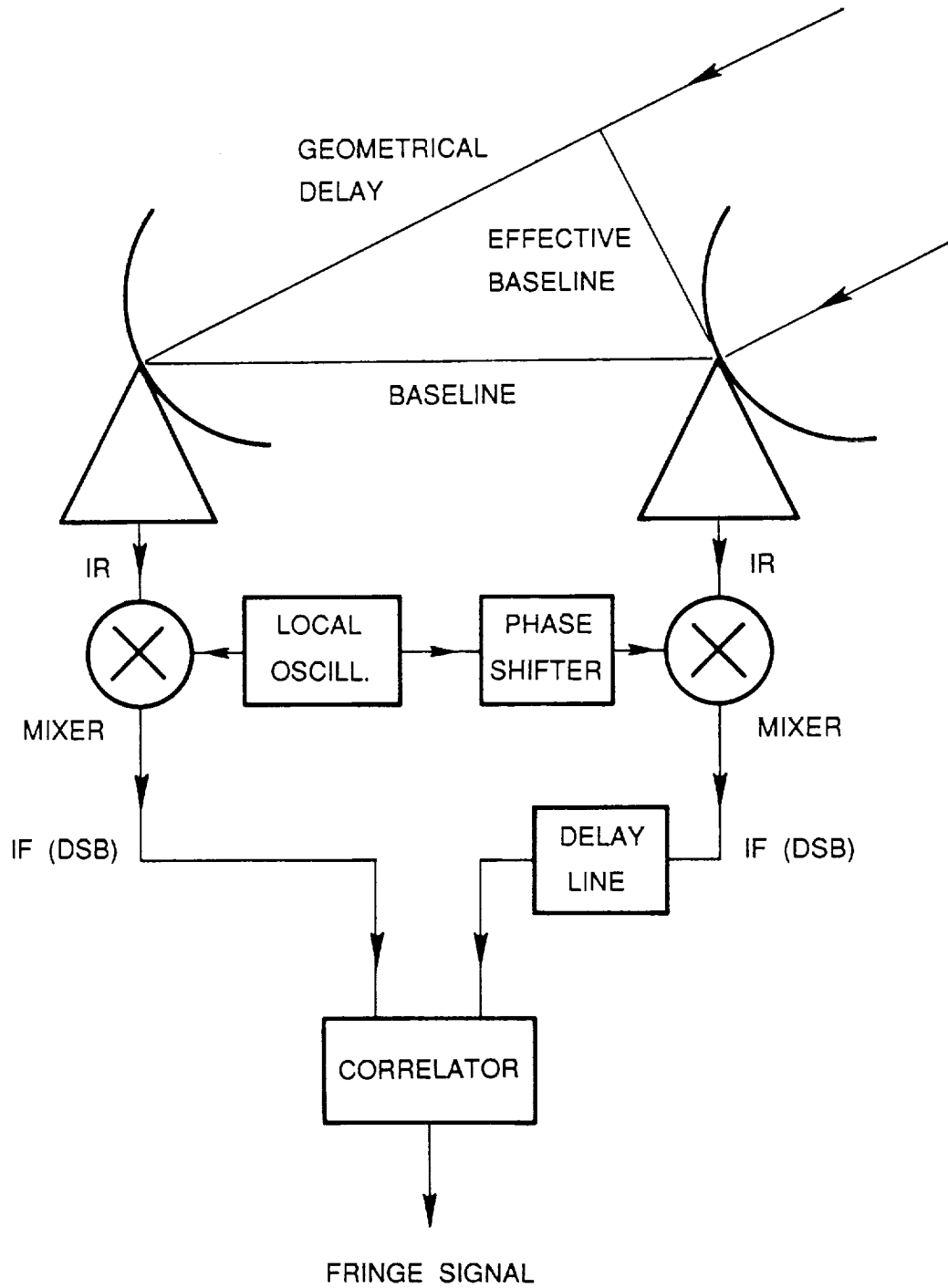


Figure 2: Schematic illustration of the basic heterodyne interferometer upon which the ISI detection system is based.

Danchi et al.

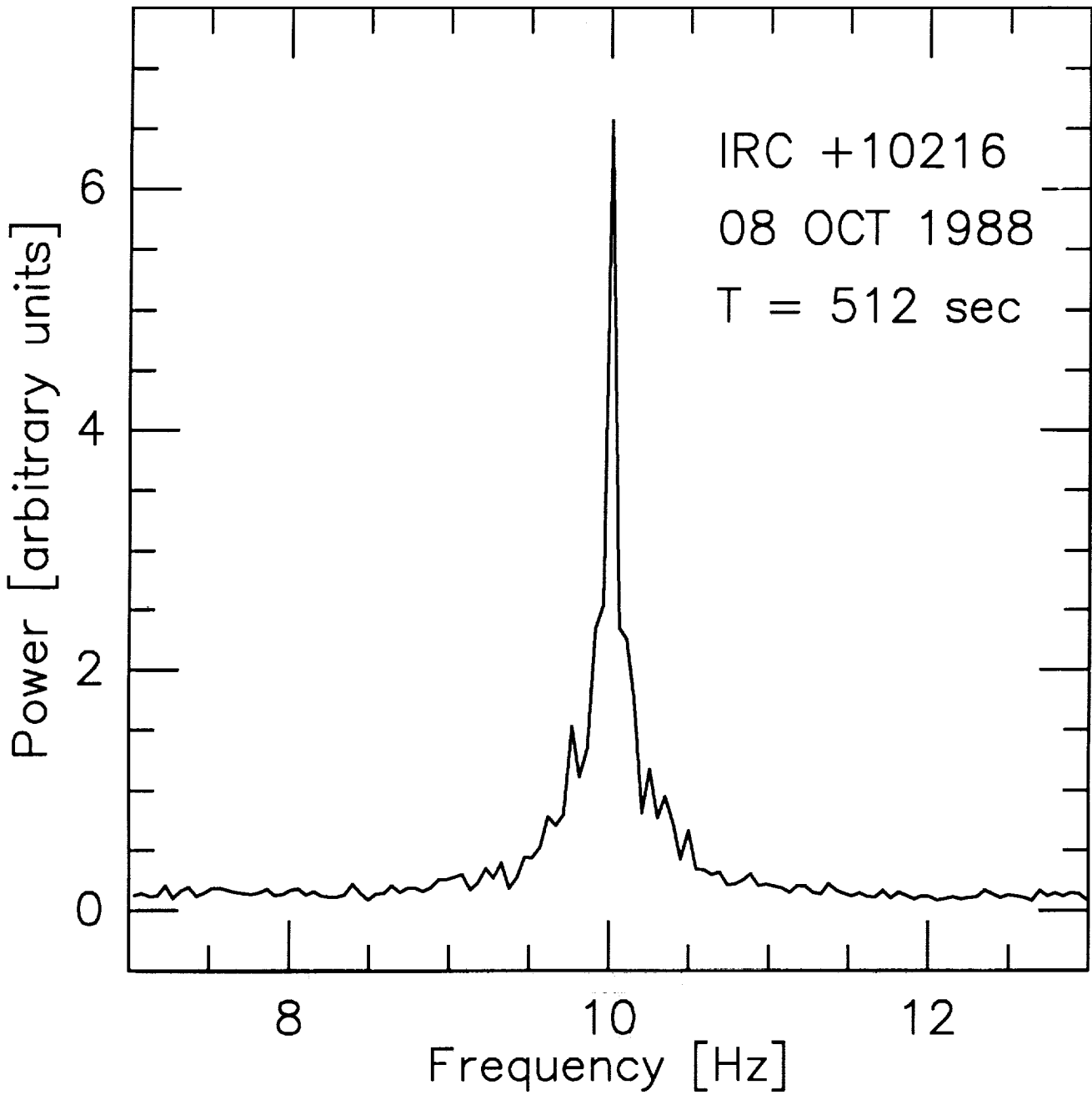


Figure 3: Power spectrum of an interference fringe obtained on IRC +10216 on 8 October 1988 after a 512-second integration time.

Danchi et al.

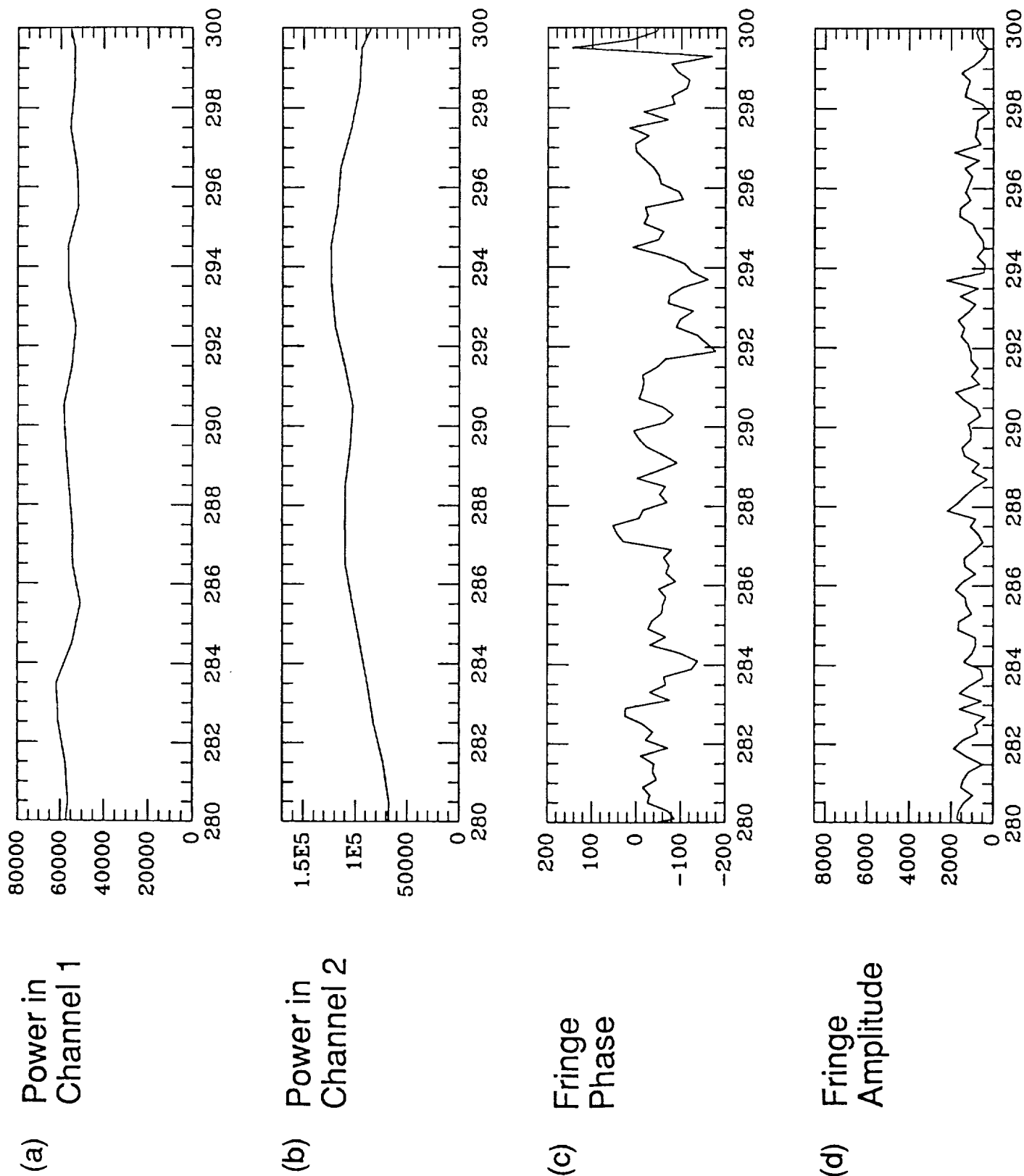


Figure 4: Infrared power in arbitrary units detected by telescope 1 (a) and by telescope 2 (b) of the ISI obtained on IRC +10216 as a function of time in seconds. (c) Phase of the interference fringe measured in degrees obtained in 0.2-second integration time periods. (d) Fringe amplitude in arbitrary units is a function of time in seconds.

Atmospheric Phase Fluctuations

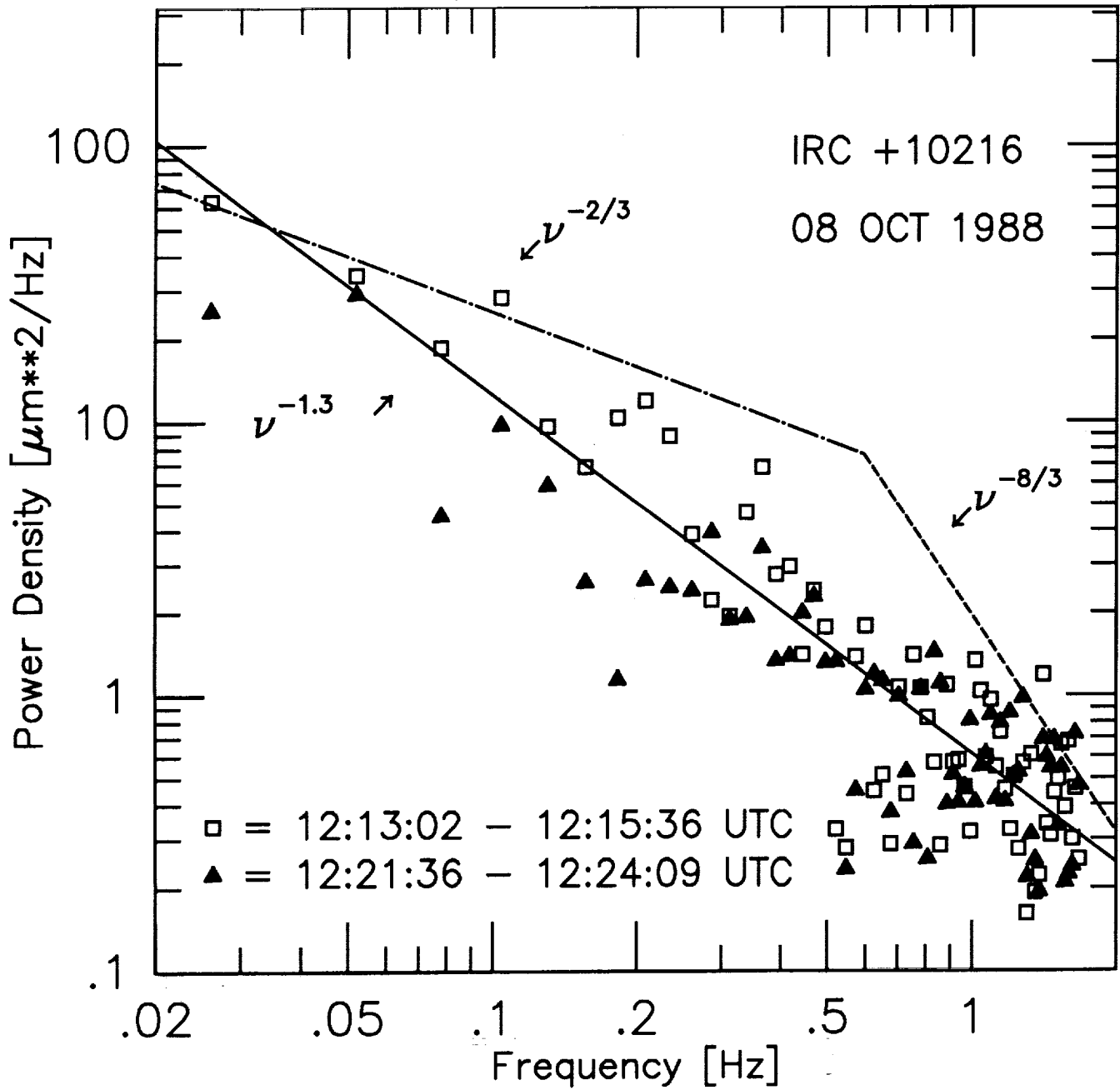
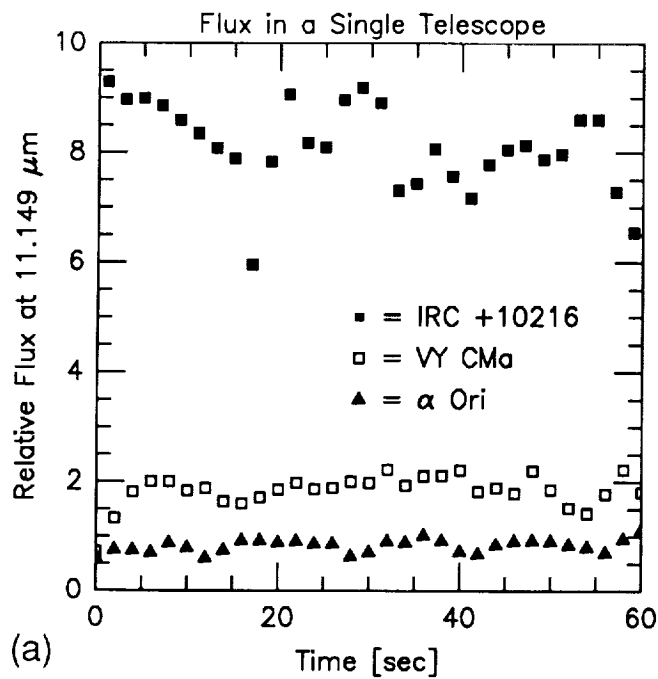
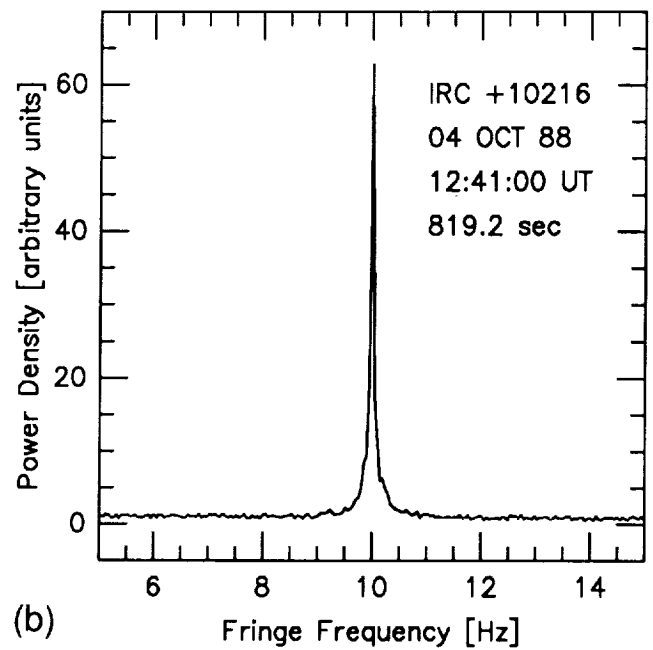


Figure 5: Power spectrum of atmospheric pathlength fluctuations obtained from data like that in figure 4. The data are from two 2.5-minute time periods. The dot-dashed line is the $\nu^{-2/3}$ asymptote and the dotted line is the $\nu^{-8/3}$ asymptote scaled for baseline differences from the data of Colavita et al. (1987).

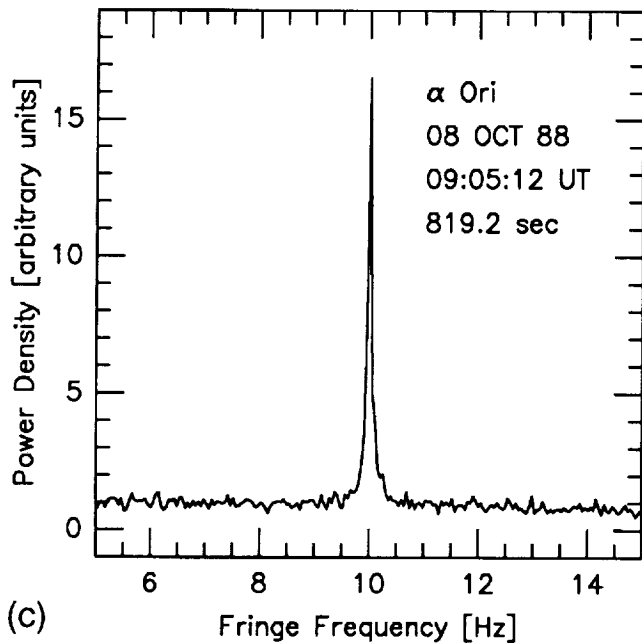
Danchi et al.



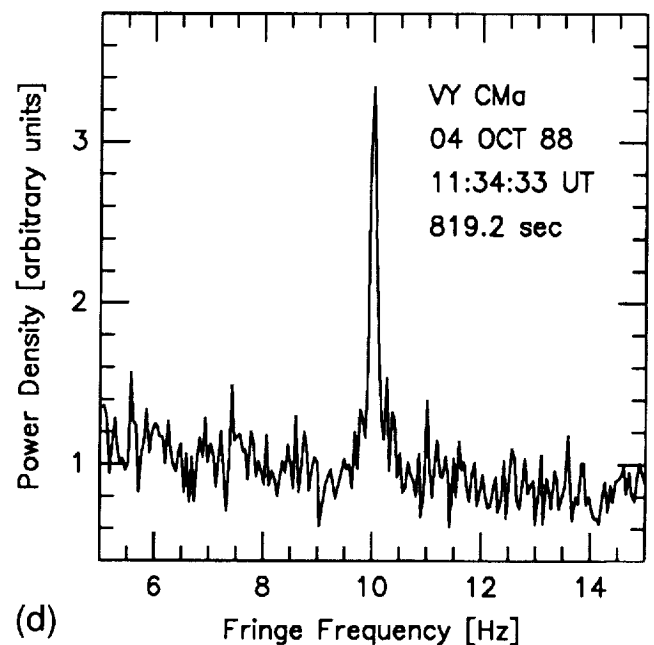
(a)



(b)



(c)



(d)

Figure 6: (a) Measured fluxes in a single telescope for IRC +10216, VY CMa, and α Ori in arbitrary units as a function of time. (b) Fringe power spectrum for IRC +10216 observed on 4 October 1988. (c) Fringe power spectrum for α Ori recorded on 8 October 1988. (d) Fringe power spectrum for VY CMa observed on 4 October 1988. Note that VY CMa has a larger single telescope flux than that of α Ori but it has less power in its interference fringes as compared to α Ori, indicating that we are resolving its dust shell.

Danchi et al.

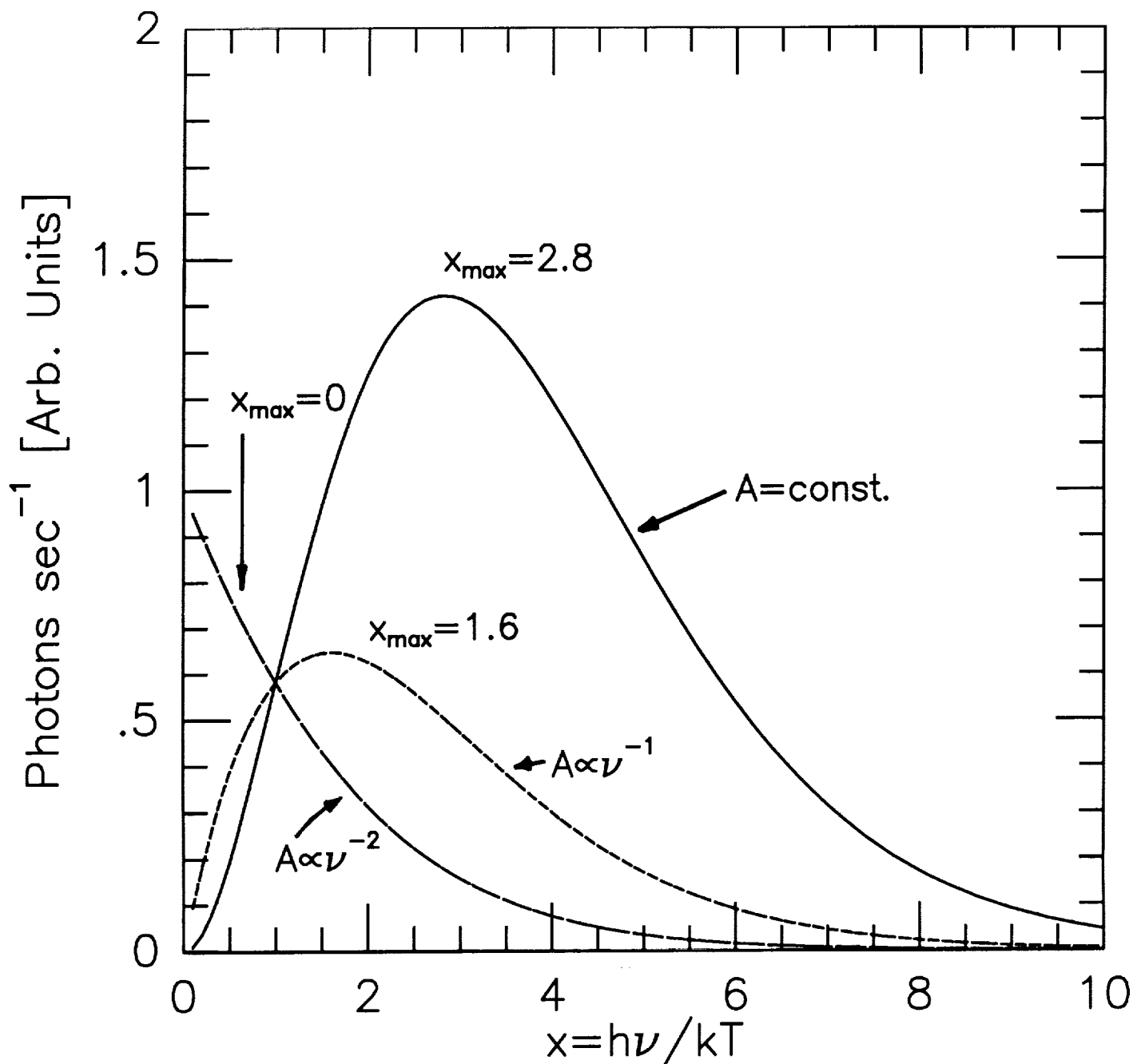


Figure 7: Number of photons per second detected by a telescope of area A with a scaling factor removed as a function of the scaled variable $x \equiv h\nu/kT$. Curves drawn are for different area (A) frequency (ν) scaling relationships, $A \propto \nu^{-n}$. The $n = 0$ case is represented by the solid line, the $n = 1$ case is drawn as the short dashed line, and the $n = 2$ case is shown by the long dashed line. Note that the maximum signal occurs at lower frequencies for a fixed temperature T as the power law index n increases.

Danchi et al.